Gas Phase Elimination Kinetics of Methyl Mandelate: Experimental and DFT Studies

Alexandra Rotinov,[†] Luz Escalante,[‡] Beatriz Ramirez,[‡] Desiree Pereira,[‡] Tania Córdova,[‡] and Gabriel Chuchani*[,†]

Centro de Química, Instituto Venezolano de Investigaciones Científicas (I.V.I.C.), Apartado 21827, Caracas, Venezuela, and Escuela de Química, Facultad de Ciencias, Universidad Central de Venezuela, Apartado 1020-A, Caracas, Venezuela

Received: February 18, 2009; Revised Manuscript Received: September 16, 2009

The gas phase elimination kinetics of racemic methyl mandelate was determined in a static system, and yielded on decomposition benzaldehyde, methanol, and carbon monoxide. The reaction was homogeneous, unimolecular, and follows a first-order law in the temperature range 379.5−440 °C and pressure range of 21.5−71.1 Torr. The variation of the rate coefficient with temperature is expressed by the following Arrhenius equation: log k_1 = (12.70 ± 0.14) − (206.5 ± 1.9) kJ/mol (2.303*RT*)$^{-1}$. The theoretical estimations of the kinetics and thermodynamics parameters were carried out using DFT methods B3LYP, B3PW91, MPW1PW91, and PBEPBE. Calculation results are in reasonably good agreement with the experimental energy and enthalpy values when using the PBEPBE DFT functional. However, regarding the entropy of activation, the MPW1PW91 functional is more adequate to describe the reaction. These calculations imply a molecular concerted nonsynchronous mechanism involving a two-step process, where the formation of the unstable α-lactone intermediate is the rate-determining factor. The lactone intermediate rapidly decarbonylates to produce benzaldehyde and carbon monoxide. The transition state is late in the reaction coordinate, resembling the lactone configuration.

1. Introduction

Work on the gas phase elimination of aliphatic alcohols has shown the OH group to be a difficult leaving group for the dehydration process. The pyrolysis of these compounds requires temperatures of 500 °C and higher for decomposition, leading to a complex reaction mechanism.[1] However, the presence of HBr or HCl as acid catalyst has been found to assist in the molecular dehydration of alcohols at lower temperatures (Scheme 1) and the activation energy is reduced by more than 100 kJ/mol.[1–3] In association with this intermolecular acid catalysis, the thought of intramolecular acid hydrogen participation led us to examine the elimination kinetics of primary, secondary, and tertiary α-hydroxycarboxylic acids in the gas phase.[4] According to product formation and kinetic parameters, the mechanism was believed to occur in terms of a semipolar five-membered cyclic transition state where C−OH bond polarization, in the sense $C^{\delta+}\cdots O^{\delta-}$, is rate determining. The intermediate lactone, unstable under experimental conditions, decomposes into the corresponding carbonyl compound and CO gas (reaction 1).

The idea for an effective assistance of the acidic hydrogen of the COOH group to a faster dehydration process suggested the study of the gas phase elimination kinetic of mandelic acid.[5] This substrate was shown to be about 20 times faster in H_2O elimination than lactic acid. The mechanism was considered to be that described in reaction 1. These experimental works led to examination of the potential energy surface (PES) at different levels of quantum chemical calculations for understanding the nature of the molecular mechanism of the gas phase molecular elimination of the 2-hydroxycarboxylic acid and mandelic acid.[6,7] Quantitative agreement was obtained between the theoretical and experimental results, but with a small mechanistic modification associated to water elimination of the α-lactone intermediate, by means of the nucleophilic attack by the carbonyl oxygen atom (Scheme 2).

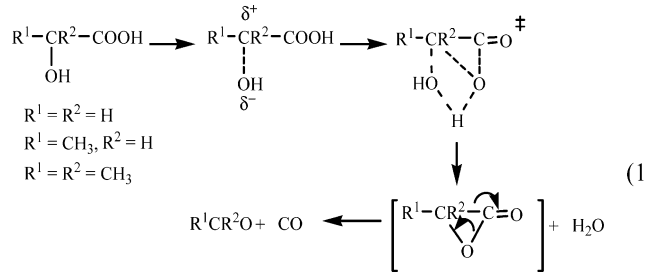

(1)

Along this type of investigation, a joint experimental and theoretical study on the mechanisms of the methyl ester of 2-hydroxycaboxylic acids, that is, methyl 2-hydroxypropionate and methyl 2-hydroxyisobutyrate, in the gas phase was reported.[8]

SCHEME 1

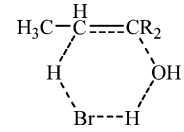

SCHEME 2

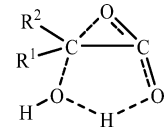

* Corresponding author, chuchani@ivic.ve.
[†] Centro de Química, Instituto Venezolano de Investigaciones Científicas (I.V.I.C.).
[‡] Escuela de Química, Facultad de Ciencias, Universidad Central de Venezuela.

10.1021/jp9046424 CCC: $40.75
Published on Web 10/05/2009

The reaction mechanisms were theoretically characterized at B3LYP/6-31+G**, MP2/ 6-31+G**, and MP2/ 6-31++G** computing levels, with the result that the reaction proceeds via a concerted, asynchronous, five-membered cyclic transition state structure. The extension of the O−H bond with subsequent migration of the H of the oxygen carbonyl appears to be the driving force for the elimination process (reaction 2). Calculated thermodynamic and kinetic parameters were found to be in good agreement with the experimental values.

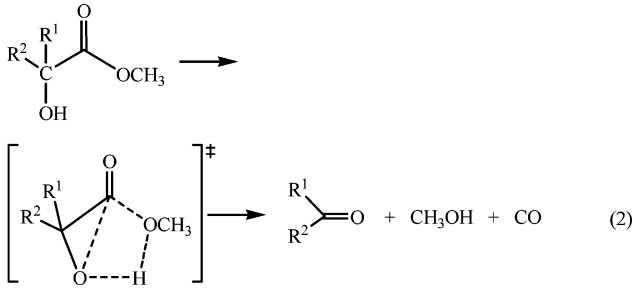

(2)

A significant difference in rate of elimination has been found between 2-hydroxypropionic acid (lactic acid) and 2-hydroxyisobutyric acid, while little difference in rates was found with their corresponding methyl esters.[4,8] In addition to this fact, mandelic acid, a secondary hydroxy acid, decarbonylates faster when compared to 2-hydroxypropionic acid (lactic acid).[5] Consequently, the present work studied the experimental gas phase elimination kinetics of methyl mandelate and also carried out a detailed theoretical study of the corresponding reaction mechanism. In this respect, we expect to obtain a more reasonable mechanism of methyl ester in 2-hydroxycarboxylic acid thermal elimination and also to compare experimental and theoretical values of the activation parameters.

2. Experimental Section

Racemic methyl mandelate (99%) was bought from Aldrich. The identification and purity of this substrate were verified by GC-MS (Saturn 2000, Varian), with a DB-5MS capillary column 30 m × 0.25 mm. i.d., 0.25 μm film thickness. The identification analyses of the products benzaldehyde (Merck) and methanol (Merck) were carried out by using the same GC-MS (Saturn 2000, Varian). The product benzaldehyde was quantitatively analyzed using a Hewlett-Packard model 5710-A chromatograph with a flame ionization detector and a 2 m packed column of 7% FFAP, Chromosorb WAW DMCS 80/100 mesh. For the quantitative analysis of the other product methanol (Fisher), a Varian 3700 gas chromatograph with a Porapak R column (80−100 mesh) was used.

Kinetics. The kinetics experiments were carried in a static reaction system as previously reported.[9−11] The reaction vessel was deactivated by the decomposition products of allyl bromide. The rate coefficients were determined manometrically or by the quantitative GC analyses of the corresponding products benzaldehyde and/or methanol. The temperature was controlled by a Shinko DC-PS resistance thermometer controller, maintained at ±0.2 °C and measured with a calibrated platinum/platinum−13% rhodium thermocouple. No temperature gradient was observed along the reaction vessel. The starting materials were dissolved in dioxane and injected directly into the reactor with a syringe through a silicone rubber septum. The amount of substrate used for each reaction was ∼0.05−0.2 mL.

TABLE 1: Ratio of Final (P_f) to Initial Pressure (P_0) of the Substrate

substrate	temp (°C)	P_0 (Torr)	P_f (Torr)	P_f/P_0	av
methyl mandelate	410.5	38.7	122.7	3.2	3.3 ± 0.1
	420.2	38.2	124.2	3.3	
	429.4	37.5	123.0	3.3	
	440.2	24.8	81.8	3.3	

3. Computational Methods and Models

The potential energy surface in the region encompassing the methyl mandelate and products benzaldehyde, methanol, and carbon monoxide was explored using density functional theory methods B3LYP, B3PW91, MPW1PW91, and PBEPBE levels of theory with basis set 6-31G, 4-31G(d) and 6-31G(d), 6-31G(d, p), and 6-31+G(d), as implemented in Gaussian 03W.[12] The transition state search was performed using quadratic synchronous transit protocol. The nature of stationary points was established by calculating and diagonalizing the Hessian matrix (force constant matrix). Transition state (TS) structures were characterized by means of normal-mode analysis. The unique imaginary frequency associated with the transition vector (TV), i.e., the eigenvector associated with the unique negative eigenvalue of the force constant matrix, has been obtained. Intrinsic reaction coordinate (IRC) calculations were performed to verify that the transition state structures connect the reactant and products in the reaction path. Calculations were performed for the rate-determining step as well as the fast step.

Thermodynamic quantities such as zero point vibrational energy (ZPVE), temperature corrections ($E(T)$), and absolute entropies ($S(T)$) were obtained from frequency calculations. Temperature corrections and absolute entropies were obtained assuming ideal gas behavior from the harmonic frequencies and moments of inertia by standard methods at average temperature and pressure values within the experimental range.[13] Scaling factors for frequencies and zero point energies for the B3LYP method used are taken from the literature.[14] In the case of DFT functionals B3PW91, PW1PW91, and PBEPBE, the B3LYP scaling factor was used.[14]

The first-order rate coefficient $k(T)$ was calculated using the transition state theory (TST)[15] and assuming that the transmission coefficient is equal to 1, as expressed in

$$k(T) = (K_B T/h) \exp(-\Delta G^{\#}/RT)$$

where $\Delta G^{\#}$ is the Gibbs free energy change between the reactant and the transition state and K_B and h are Boltzmann and Plank constants, respectively.

$\Delta G^{\#}$ was calculated using the following relations

$$\Delta G^{\#} = \Delta H^{\#} - T\Delta S^{\#}$$

$$\Delta H^{\#} = V^{\#} + \Delta\text{ZPVE} + \Delta E(T)$$

where $V^{\#}$ is the potential energy barrier and ΔZPVE and $\Delta E(T)$ are the differences of ZPVE and temperature corrections between the TS and the reactant, respectively. Entropy values were calculated from vibrational analysis.

4. Results and Discussion

4.1. Experimental Results. The unimolecular elimination of racemic methyl mandelate in the gas phase is described by

TABLE 2: Stoichiometry of the Reaction

substrate	temp (°C)	parameter	value				
methyl mandelate	390.3 ± 0.2	time (min)	10	20	30	40	50
		reaction (%) (pressure)	15.4	23.1	34.5	45.6	67.2
		benzaldehyde (%) GLC)	15.7	21.2	36.0	47.8	67.7
		methanol (%) GLC	14.9	22.3	33.4	45.1	65.6

TABLE 3: Homogeneity of the Elimination Reactions

substrate	S/V (cm^{-1})[a]	10^4k_1 (s^{-1})[b]	10^4k_1 (s^{-1})[c]
methyl mandelate at 410.5 °C	1	9.01 ± 0.39	8.47 ± 0.28
	6	11.24 ± 0.46	8.72 ± 0.24

[a] Key: S = surface area; V = volume. [b] Clean Pyrex vessel. [c] Vessel seasoned with allyl bromide.

TABLE 4: Effect of Free Radical Inhibitor Toluene on Rates[a]

substrate	temp (°C)	P_s (Torr)	P_i (Torr)	P_i/P_s	10^4k_1 (s^{-1})
methyl mandelate	429.4	37.7			22.64 ± 0.16
		53.3	54	1.0	22.25 ± 0.14
		42.6	90	2.1	23.01 ± 0.21
		36.6	113.5	3.0	22.23 ± 0.19

[a] P_s = pressure substrate. P_i = pressure inhibitor.

reaction 1. The stoichiometry of reaction 1 demands for a long reaction time $P_f/P_0 = 3.0$, where P_f and P_0 are the final and initial pressures, respectively. The average experimental P_f/P_0 at four different temperatures and 10 half-lives was 3.3 (Table 1). Since very little benzene was detected in product formation, the departure from theoretical stoichiometry may be due to a small decomposition of the product benzaldehyde into benzene and CO gas. However, stoichiometry of reaction 1, up to 67% decomposition, was verified by comparing the extent of

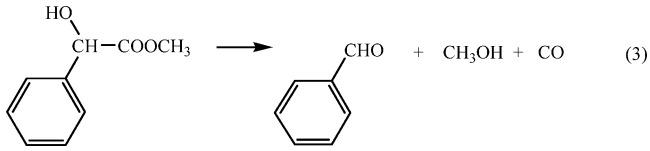

(3)

decomposition of the substrate from pressure measurements with that obtained from quantitative GLC analyses of benzaldehyde and methanol formations (Table 2).

The homogeneity of the elimination was examined by using a reaction vessel with different surface-to-volume ratio. That is, the packed vessel has a 6 times greater surface-to-volume ratio than the unpacked vessel (Table 3). The packed and unpacked clean Pyrex vessels had a small but significant effect on the rates. However, the packed and unpacked Pyrex vessels seasoned with allyl bromide had no effect on rates.

The effect of different proportions of free radical inhibitor toluene had no effect on the rates (Table 4). No induction period was observed and the rates were reproducible with a relative standard deviation of not greater than 5% at a given temperature.

The rate coefficients for elimination, calculated from $k_1 = (2.303/t) \log[2P_0/(3P_0 - P_t)]$, are invariable to initial pressures (Table 5), and the first order plots of $\log(3P_0 - P_t)$] against time t gave a good straight line for up to 65% decomposition. The variation of the rate coefficients with temperature and the corresponding Arrhenius equation are given in Table 6, where 90% confidence limits from a least-squares procedure are given.

The comparative kinetic and thermodynamic parameters of methyl mandelate with respect to methyl 2-hydroxypropionate and methyl 2-hydroxyisobutyrate are described in Table 7.[8] The parameters were calculated using the relation $\Delta H^{\ddagger} = E_a - nRT$, the Arrhenius equation $k = Ae^{-E_a/RT}$, and the Eyring equation $k = k_B T/h e^{-\Delta G^{\neq}/RT}$, $\Delta S^{\ddagger} = [\ln A - \ln(e^n k_B T/h)]R$. The kinetic and thermodynamic parameters of methyl mandelate were found constant within the experimental temperature range.

4.2. Theoretical Results. ***4.2.1. Kinetic and Thermodynamic Parameters.*** The gas phase elimination path of methyl mandelate to give benzaldehyde, methanol, and carbon monoxide was studied using different DFT methods. From the experimental results, the formation of benzaldehyde, methanol, and carbon monoxide was explained as in reaction 8. The section of the potential energy surface between the reactant and products was explored to obtain reasonable structures for reactant, products, and the transition state, which account for the experimental parameters observed.

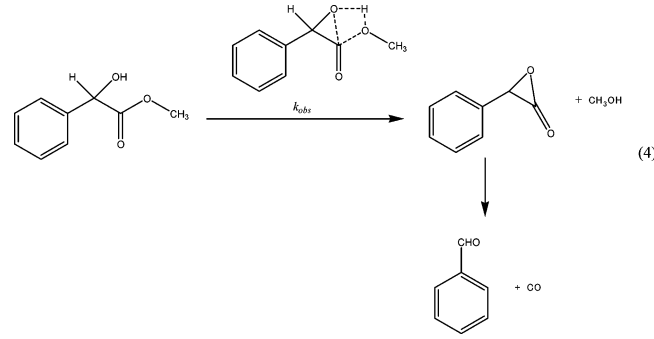

(4)

Calculation results illustrate that the mechanism for decomposition involves a slow step with the formation of methanol and the unstable α-lactone intermediate, which rapidly decarbonylates to give benzaldehyde and carbon monoxide. Essentially, the same structures are obtained in all DFT methods.

IRC calculations demonstrated that the TS structure connects the reactant methyl mandelate and products methanol and the α-lactone intermediate. Calculations showed that the reaction path through a three-membered ring transition state structure resembling the lactone intermediate is unique to the formation of the above-mentioned products from methyl mandelate; that is, the calculated TS leads to methyl mandelate in the reverse direction and to the products lactone intermediate and methanol, in the forward direction.

Calculated kinetic and thermodynamic parameters for the decomposition of methyl mandelate to give methanol and the α-lactone are shown in Table 7. Theoretical results for the rate-determining step from calculation at different levels of theory for the energy of activation, enthalpy, and free energy of activation, showed a better accord to experimental values when using the DFT functional PBEPBE. Other DFT functionals B3LYP, B3PW91, and MPW1PW91 overestimate the reaction barrier. The use of bigger basis set did not improve the results.

Conversely, for the entropy of activation, the experimental results are better reproduced with the MPW1PW91 functional. The observed negative value for entropy of activation about −17 kJ/(mol K) suggests the loss of degrees of freedom in the TS in the rate-determining step implying a somehow rigid structure.

TABLE 5: Invariability of the Rate Coefficients with Initial Pressure

substrate	temp (°C)	parameters	value			
methyl mandelate	429.4	P_0 (Torr)	21.5	30.4	53.3	71.1
		$10^4 k_1$ (s^{-1})	22.34 ± 0.21	22.50 ± 0.16	22.25 ± 0.11	22.43 ± 0.16

TABLE 6: Variation of Rate Coefficient with Temperature in Methyl Mandelate

temp (°C)	379.5	390.3	399.2	410.5	420.0	429.4	440.0
$10^4 k_1$ (s^{-1})	1.50	2.75	4.51	8.47	13.49	22.51	37.60

rate of equation $\log k_1 = (12.70 \pm 0.14) - (206.5 \pm 1.9)$ kJ/mol $(2.303RT)^{-1}$, $r = 0.9999$

The study of the subsequent decarbonylation step of the lactone intermediate was also carried out to confirm the nature of the rate-determining step. Thermodynamic parameters of the lactone decomposition step are relative to the lactone intermediate. The results are given in Table 9 together with the thermodynamics parameters for the first step for comparison purposes.

For the decarbonylation step the potential barrier was found to be 115.76 kJ/mol^{-1} at the PBEPBE/6-31G level of theory, in contrast to the value for the first step of 206.9 kJ/mol. Free energies of activation also show the same trend, implying that the second step or lactone decomposition is more facile than the preceding step. In both steps, there is a higher enthalpy contribution to the Gibbs free energy. The entropy of activation for the second step is less negative suggesting less reorganization going from the lactone intermediate to the TS in the second step. This result confirms that the rate-determining step of the gas-phase thermal decomposition of methyl mandelate is the formation of methanol and the α-lactone intermediate. The transition state structure for the lactone formation step was verified by IRC calculations, thus confirming that the TS led to the products of the first step (forward direction) and reactant (reverse direction).

4.2.2. Transition State and Mechanism. The transition state structure is characterized by the vector linked with the unique imaginary frequency. This vector is associated with the hydrogen migration of the OH to the oxygen of the OCH_3 and is also related to α-lactone formation, i.e., the translation of the hydroxyl oxygen O5 approaching the carbonyl carbon C1 (Scheme 3, Figure 1). Structural parameters for reactant methyl mandelate (R), the transition state (TS), and products methanol and α-lactone intermediate (P) are given in Table 10 using MPW1PW91, because the entropy of activation was better reproduced using this method.

Variation in bond distances, bond angles, and dihedrals can be used to follow the reaction progress from the reactant to the transition state structure to products of the rate-determining step. On average, the transition state geometry for the rate-determining step is closer to the α-lactone intermediate than to the reactant. The TS structure shows a three-membered ring configuration, involving atoms C1, C3, O5. One process occurring in the rate-determining step is the migration of hydrogen H6 from O5 to O18 to form methanol. The hydrogen being transferred, H6, is closer the ester oxygen O18 than the hydroxyl oxygen O5 in the TS implying important progress in this reaction coordinate (Scheme 3, Figure 1). The C3−O5 distance in the TS is close to that in the reactant. Conversely, the O5−C1 distance has decreased in the TS showing that the hydroxyl oxygen is closer to the carbonyl carbon C1 to form the α-lactone.

The O5−C1 bond distance is 2.434 Å in the reactant and changes to 1.818 Å in the TS as the α-lactone intermediate is being formed. In the intermediate the O5−C1 distance is 1.366 Å. The progress in C1−O18 bond breaking is evident from the changes in distances from 1.366 to 1.930 Å in the TS. Elongation of O5−H6 bond from 0.977 to 1.743 Å occurs together with the formation of H6−O18 bond which changes from 2.087 to 1.010 Å. The unique imaginary frequency in the TS is associated with oxygen O3 moving toward carbon C1 to form the lactone intermediate and also with the hydrogen transfer from O3 to O18.

NBO analysis was used to study the electron density redistribution in the reaction path of methyl mandelate thermal decomposition. Table 11 displays NBO charges for the reactant (R), transition state (TS), and the lactone intermediate (P).

In the rate-determining step leading to α-lactone intermediate, small changes in NBO charges are observed. There is a decrease in electron density at O5 from the reactant to the transition state (−0.615 to −0.574) while C1 becomes less positively charged (0.563−0.482) suggesting a displacement of electron density from O5 to C1 as the lactone TS is formed. Other changes in electron density are minor.

4.2.3. Natural Bond Orbital (NBO). The reaction progress along the reaction pathway was also investigated by means of NBO bond order calculations.[16–18] Wiberg bond indexes[19] were computed using the NBO program[20] as implemented in Gaussian 03W. These indexes can be used to estimate bond orders from population analysis. Bond breaking and bond making processes involved in the reaction mechanism are monitored by means of the Synchronicity (Sy) concept proposed by Moyano et al.[21] defined by the expression

$$\mathrm{Sy} = 1 - [\sum_{i=1}^{n} |\delta B_i - \delta B_{\mathrm{av}}| / \delta B_{\mathrm{av}}] / 2n - 2$$

n is the number of bonds directly involved in the reaction and the relative variation of the bond index is obtained from

$$\delta B_i = [B_i^{\mathrm{TS}} - B_i^{\mathrm{R}}] / [B_i^{\mathrm{P}} - B_i^{\mathrm{R}}]$$

where the superscripts R, TS, and P represent reactant, transition state, and product, respectively.

The evolution in bond change is calculated as

$$\% \mathrm{Ev} = \delta B_i \times 100$$

The average value is calculated from

$$\delta B_{\mathrm{av}} = 1/n \sum_{i=1}^{n} \delta Bi$$

Changes along the reaction coordinate were followed using Wiberg bonds indexes B_i. The indexes were calculated for those bonds involved in the reaction changes, i.e., C3−O5, O5−C1, O5−H6, H6−O8, and O18−C1 (Scheme 3, Table 12). All other bond bonds remain practically unaffected during the process.

TABLE 7: Comparative Kinetic and Thermodynamic Parameters at 400 °C

compound	$10^4 k_1$ (s^{-1})	E_a (kJ/mol)	log A (s^{-1})	$\Delta S^{\ddagger}$ (J/(mol K))	$\Delta H^{\ddagger}$ (kJ/mol)	$\Delta G^{\ddagger}$ (kJ/mol)
methyl mandalate[a]	4.70	206.5 ± 1.9	12.70 ± 0.14	–17.0	200.9	212.4
methyl 2-hydroxypropionate[b]	4.79	219.8 ± 2.5	13.73 ± 0.19	2.85	214.2	212.3
methyl 2-hydroxyisobutyrate[b]	3.39	217.1 ± 5.1	13.37 ± 0.39	–4.04	211.5	214.2

[a] This work. [b] Reference 8.

TABLE 8: Calculated Kinetic and Thermodynamic Parameters Obtained for the Rate-Determining Step of the Elimination Reaction of Methyl Mandelate at 400 °C and 0.0487 atm

methods	$\Delta H^{\ddagger}$ (kJ/mol)	$\Delta G^{\ddagger}$ (kJ/mol)	$\Delta S^{\ddagger}$ (J/(mol K))	E_a (kJ/mol)	log A	$10^{-4} k$ (s^{-1})
B3LYP/6-31G	237.8	240.98	–4.64	243.49	13.35	0.053
B3LYP/6-31G(d)	244.9	239.98	7.21	250.58	13.96	0.0019
B3LYP/4-31G(d)	242.6	244.1	–2.21	248.32	13.47	0.00096
B3LYP/6-31G(d,p)	283.3	304.10	–30.52	288.94	11.99	0.00000014
B3LYP/6-31+G(d,p)	247.2	236.0	16.43	252.86	14.45	0.0038
B3PW91/6-31G	239.1	244.33	–7.67	244.78	13.19	0.0296
MPW1PW91/6-31G	248.2	260.22	–17.65	253.84	12.67	0.000052
PBEPBE/6-31G	201.2	210.54	–13.63	206.91	12.88	0.63
PBEPBE/6-31G(d)	210.5	214.43	–5.73	216.19	13.29	0.28
PBEPBE/4-31G(d)	208.3	211.5	–4.69	213.93	13.34	0.49
exptl	200.9	212.4	–17.0	206.5	12.70	8.13

TABLE 9: Thermodynamic Parameters for the First Step (Latone Formation) and Second Step (Decarbonylation) of the Elimination Reaction of Methyl Mandelate at 410 °C and 0.0487 atm, Calculated Using PBEPBE/6-31G Level of Theory

	$\Delta H^{\ddagger}$ (kJ/mol)	$\Delta G^{\ddagger}$ (kJ/mol)	E_a (kJ/mol)	$\Delta S^{\ddagger}$ (kJ/K mol)
first step	201.2	210.5	206.9	−13.63
second step	110.1	112.9	115.8	−4.13
experimental	200.8	212.4	206.5	−16.99

SCHEME 3

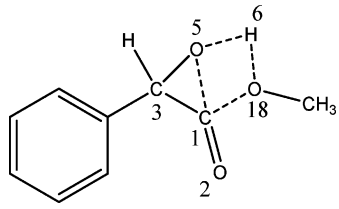

Analysis of Wiberg bond indexes shows that the most advanced reaction coordinate is the migration of hydrogen H6 as seen in the progress of O5−H6 bond breaking (85.07%) and the H6−O18 bond formation (80.32%). The breaking of O18−C1 is also important (66.47%) while O5−C1 is less than half way in the reaction coordinate (46.04%). Changes in C3−O5 are small in the TS. The synchronicity parameter Sy = 0.7603 suggests a polar, asynchronic process, with a late TS in the sense of the hydrogen transfer from the hydroxyl moiety. The TS structure resembles the α-lactone intermediate.

5. Conclusions

The thermal decomposition of methyl mandelate to benzaldehyde, methanol, and carbon monoxide was found to be homogeneous, unimolecular, and follow a first-order kinetics. No surface effects were observed. The variation of the rate coefficient with temperature gives an Arrhenius expression: log $k_1 = (12.70 \pm 0.14) - (206.5 \pm 1.9)$ kJ/mol $(2.303\ RT)^{-1}$.

The potential energy surface along the reaction path was studied by means of electronic structure calculations at different theory levels. We found that DFT functional PBEPBE produced the better agreement for enthalpy of activation and consequently the activation energy, when compared to the experimental results. The other DFT methods overestimate the reaction barrier. The PBE functional is a derivation of GGA with construction underlying PW91 GGA functional.[22] PBEPBE is

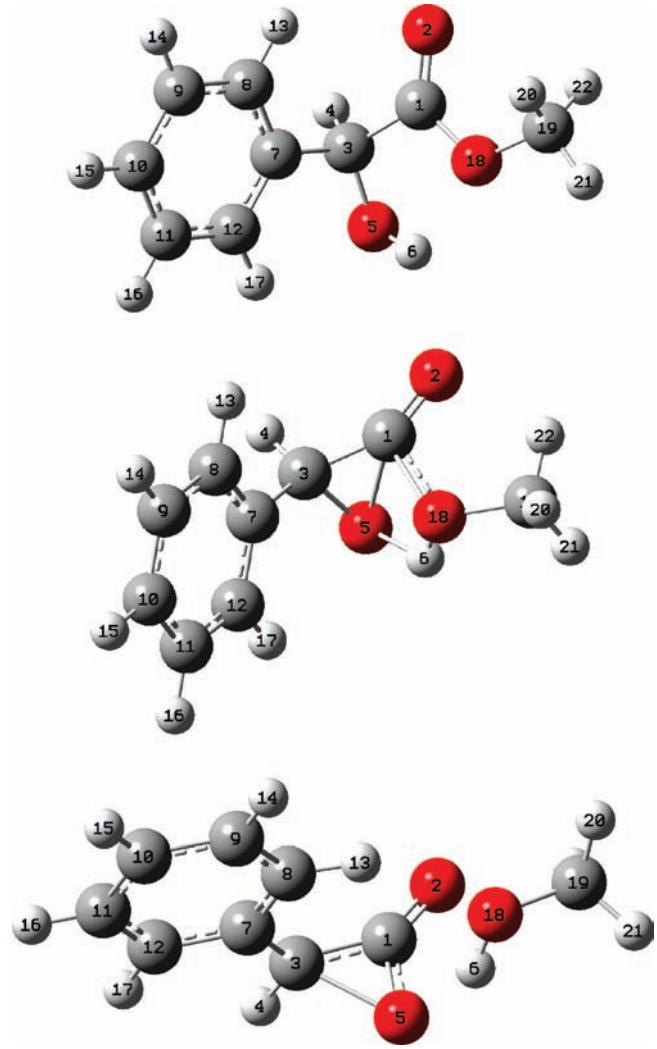

Figure 1. Optimized structures for reactant methyl mandelate (top), transition state (center), and products methanol and the α-lactone intermediate (bottom) at the PBEPBE/6-31G level of theory. The TS geometry resembles the lactone product.

TABLE 10: Structural Parameters for Reactant (R), Transition State (TS), and Products for Methyl Mandelate Thermal Decomposition from MPW1PW91/6-31G Calculations[a]

Atom Distances (Å)						
structure	C3−O5	O5−C1	C3−C1	O5−H6	H6−O18	O18−C1
R	1.434	2.434	1.516	0.977	2.087	1.366
TS	1.494	1.818	1.453	1.743	1.010	1.930
P	1.667	1.366	1.458	2.067	0.976	3.197

Dihedrals		
	O18−C1−C3−O5	C1−O18−H6−O5
reactant	–27.26	10.99
transition State	–71.37	–8.66
product	–56.57	–121.50

Imaginary Frequency (cm^{-1})
357.01

[a] Atom distances are in angstroms; bond and dihedral angles are in degrees.

TABLE 11: NBO Charges of the Atoms Involved in Methyl Mandelate Thermal Decomposition from MPW1PW91/6-31G Calculations

	C3	C1	O18	H6	O5
reactant	–0.047467	0.563415	–0.552270	0.401124	–0.615256
transition state	–0.066401	0.482446	–0.604684	0.434517	–0.574185
product	–0.169734	0.509703	–0.660442	0.401908	–0.450378

TABLE 12: NBO Analysis for Methyl Mandelate Thermal Decomposition[a]

structure	C3−O5	O5−C1	O5−H6	H6−O18	O18−C1
δBR	0.9617	0.0338	0.7302	0.0146	1.0389
δBTS	0.9141	0.5273	0.138	0.5765	0.3529
δBP	0.6428	1.1057	0.0341	0.7142	0.0069
%Ev	14.93	46.04	85.07	80.32	66.47
	δB_{av} 0.5857			Sy = 0.7603	

[a] Wiberg bond indexes (B_i) and % evolution through the reaction coordinate (%Ev) are shown for R, TS, and P. Average bond index variation (δB_{av}) and synchronicity parameter (Sy) are also reported.

improved over PW91 and retains some features of LSD and combines them with the more energetically favored features of gradient-corrected nonlocality. It appears that the contribution of local varying density in the TS is important in the thermal decomposition of methyl mandelate. However, we have observed that regarding the entropy of activation, the MPW1PW91 functional is more adequate to describe the reaction.

Even though experimental results gave benzaldehyde, methanol, and carbon monoxide as decomposition products of methyl mandelate elimination, the theoretical studies suggest that the reaction occurs in two steps. The rate-determining step involves the formation of α-lactone intermediate and methanol. The intermediate is unstable at the reaction conditions and further decarbonylates to give benzaldehyde and carbon monoxide. The TS of the first step is a three-membered ring that resembles the lactone intermediate. The observed TS structure differs from that suggested in a previous study,[7] by proposing a nucleophilic attack of the hydroxyl oxygen on the ester carbonyl carbon in the rate-determining step, as previously proposed by Chuchani et al.[5] NBO bond orders suggest the reaction to proceed in a concerted polar asynchronous mechanism and that the decomposition process is dominated by the hydrogen transfer from the hydroxyl oxygen O5 to the ester oxygen O18.

Acknowledgment. One of us (T.C.) is grateful to the Consejo de Desarrollo Científico y Humanístico (C.D.C.H.) for Grant No. PG-03-00-6499-2006.

References and Notes

(1) Failes, F. L.; Shapiro, J. S.; Stimson, V. R. *Chemistry of Ethers, Crown Ethers, Hydroxyl Groups and their Sulfur Analogues*; Patai, S., Ed.; Wiley: Chichester, 1980; Vol. 1, pp 449−468.
(2) Maccoll, A.; Stimson, V. R. *J. Chem. Soc.* **1960**, 2836–2841.
(3) Chuchani, G.; Dominguez, R. M.; Rotinov, A.; Martin, I. *React. Kinet. Catal. Lett.* **1991**, *45*, 291–297.
(4) Chuchani, G.; Martin, I.; Rotinov, A.; Dominguez, R. M. *J. Phys. Org. Chem.* **1993**, *6*, 54–58.
(5) Chuchani, G.; Martin, I. *J. Phys. Org. Chem.* **1997**, *10*, 121–124.
(6) Domingo, L. R.; Andrés, J.; Moliner, V.; Safont, V. S. *J. Am. Chem. Soc.* **1997**, *119*, 6415–6422.
(7) Domingo, L. R.; Pitcher, M. T.; Andres, J.; Safont, V. S.; Chuchani, G. *Chem. Phys. Lett.* **1997**, *274*, 422–428.
(8) Safont, V. S.; Andrés, J.; Castillo, R.; Chuchani, G.; Rotinov, A.; Domínguez, R. M.; Herize, A. *J. Phys. Chem. A* **2004**, *108*, 996–1007.
(9) Maccoll, A. *J. Chem. Soc.* **1955**, 965–973.
(10) Swinbourne, E. S. *Aust. J. Chem.* **1958**, *11*, 314–330.
(11) Dominguez, R. M.; Herize, A.; Rotinov, A.; Alvarez-Aular, A.; Visbal, G.; Chuchani, G. *J. Phys.Org. Chem.* **2004**, *17*, 399–408.
(12) Frisch, M. J.; Trucks, G. W.; Schlegel, H. B.; Scuseria, G. E.; Robb, M. A.; Cheeseman, J. R.; Montgomery, J. A., Jr.; Vreven, T.; Kudin, K. N.; Burant, J. C.; Millam, J. M.; Iyengar, S. S.; Tomasi, J.; Barone, V.; Mennucci, B.; Cossi, M.; Scalmani, G.; Rega, N.; Petersson, G. A.; Nakatsuji, H.; Hada, M.; Ehara, M.; Toyota, K.; Fukuda, R.; Hasegawa, J.; Ishida, M.; Nakajima, T.; Honda, Y.; Kitao, O.; Nakai, H.; Klene, M.; Li, X.; Knox, J. E.; Hratchian, H. P.; Cross, J. B.; Bakken, V.; Adamo, C.; Jaramillo, J.; Gomperts, R.; Stratmann, R. E.; Yazyev, O.; Austin, A. J.; Cammi, R.; Pomelli, C.; Ochterski, J. W.; Ayala, P. Y.; Morokuma, K.; Voth, G. A.; Salvador, P.; Dannenberg, J. J.; Zakrzewski, V. G.; Dapprich, S.; Daniels, A. D.; Strain, M. C.; Farkas, O.; Malick, D. K.; Rabuck, A. D.; Raghavachari, K.; Foresman, J. B.; Ortiz, J. V.; Cui, Q.; Baboul, A. G.; Clifford, S.; Cioslowski, J.; Stefanov, B. B.; Liu, G.; Liashenko, A.; Piskorz, P.; Komaromi, I.; Martin, R. L.; Fox, D. J.; Keith, T.; Al-Laham, M. A.; Peng, C. Y.; Nanayakkara, A.; Challacombe, M.; Gill, P. M. W.; Johnson, B.; Chen, W.; Wong, M. W.; Gonzalez, C.; and Pople, J. A. *Gaussian 03, Revision C.02*; Gaussian, Inc., Wallingford, CT, 2004.
(13) McQuarrie, D. *Statistical Mechanics*; Harper & Row: New York, 1986.
(14) Foresman, J. B.; Frish, Æ. *Exploring Chemistry with Electronic Methods*, 2nd ed.; Gaussian, Inc.: Pittsburgh, PA, 1996.
(15) Benson, S. W. *The Foundations of Chemical Kinetics*; McGraw-Hill: New York, 1960.
(16) Lendvay, G. L. *J. Phys. Chem.* **1989**, *93*, 4422–4429.
(17) Reed, A. E.; Weinstock, R. B.; Weinhold, F. *J. Chem. Phys.* **1985**, *83* (2), 735–746.
(18) Reed, A. E.; Curtiss, L. A.; Weinhold, F. *Chem. Rev.* **1988**, *88*, 899–926.
(19) Wiberg, K. W. *Tetrahedron* **1968**, *24*, 1083–1095.
(20) Reed, A. E.; Carpenter, J. E.; Weinhold, F. *NBO version 3.1*.
(21) Moyano, A.; Periclas, M. A.; Valenti, E. *J. Org. Chem.* **1989**, *54*, 573–582.
(22) Perdew, J. P.; Burke, K.; Ernserhof, M. *Phys. Rev. Lett.* **1996**, *77* (8), 3865–3868.

JP9046424